Air pollutant sinks on noise barriers
Where do they perform the best?

Dash, Amitosh; Elsinga, Gerrit E.

DOI
10.1016/j.atmosenv.2018.05.041

Publication date
2018

Document Version
Accepted author manuscript

Published in
Atmospheric Environment

Air pollutant sinks on noise barriers: where do they perform the best?

Amitosh Dash[a,*], Gerrit E. Elsinga[a,**]

[a] *Laboratory for Aero and Hydrodynamics, Faculty of Mechanical, Maritime and Materials Engineering, Delft University of Technology, Mekelweg 2, 2628CD, Delft, The Netherlands*

Abstract

While laboratory experiments, numerical simulations as well as field tests have underlined the influence of noise barriers in dispersing vehicular emissions and reducing downwind peak concentrations, these pollutants still remain in the atmosphere. Artificial pollutant sinks (for example, particle capturing or toxic gas treating devices) installed on top of noise barriers can further alleviate this problem by eliminating the pollutants passing through it. However, it is not known how the installation of a semi-permeable pollutant sink affects the aerodynamics of the pollutants' flow. By finding an optimal position and orientation for these sinks, the mass of pollutants reaching the sink inlet can be maximized. Scaled down water tunnel experiments have been used to investigate the effectiveness of installing such a pollutant sink, of fixed dimensions, on top of a noise barrier adjacent to a highway. It is found that installing a sink is more beneficial on top of shorter barriers and that vertically elevating the sink slightly can enhance its pollutant capturing performance. Using a sink in a 'highway canyon' (two noise barriers placed symmetrically with respect to the highway) must be done cautiously as there are several flow regimes observed, which are sensitive not only to the canyon aspect ratio (ratio between canyon width and height), but also to the presence/absence of the sink. The results here not only demonstrate the effectiveness of installing pollutant sinks on noise barriers, but also provide ballpark estimates on the optimal placement, orientation and performance of these devices, prior to field tests or even large-scale installation.

Keywords: Air pollutant sinks, Laboratory scale experiments, Pollutant dispersion, Noise barrier, Highway canyon

1. Introduction

Air pollution has been a known perpetrator of reduced lifespans (World Health Organization (2006b)) for many decades now, primarily by triggering respiratory and cardiovascular diseases (Brunekreef & Holgate (2002)). Of the various constituents of air pollutants, a major component is Particulate Matter (PM). Particulate matter can be further categorized based on particle diameter into coarse (PM_{10}), fine ($PM_{2.5}$) and ultrafine particles ($PM_{0.1}$), where the subscript refers to the aerodynamic diameter of the particle in μm. Both, long term and short term exposure to these particles leads to increased mortality (Pope III et al. (2002), Pope III & Dockery (2006), Anderson et al. (2012)).

A major contributor to outdoor particulate matter is vehicular emissions (Morawska et al. (2008)). Increased urbanization is leading to the rise of rural-urban fringes, which often contain highways (Hamers et al. (2009), Nabielek et al. (2013)). The above combination leads to increased concentration of particulate matter in the urban areas closer to the source, i.e near highways and arterial roads (Morawska et al. (2008), Keuken et al. (2013)).

In order to reduce the repercussions of air pollutants on health, air quality standards were put forth (World Health

*Corresponding author
**Principal corresponding author
Email addresses: a.dash@tudelft.nl (Amitosh Dash), g.e.elsinga@tudelft.nl (Gerrit E. Elsinga)

Organization (2006a)), which in the Netherlands led to the inception of the Dutch Air Quality Innovation Program. Several solutions to mitigate air pollution were proposed and tested, one of which was the addition of Noise Barriers (NBs) next to highways (Innovatieprogramma Luchtkwaliteit (2009), Hooghwerff et al. (2010)).

Field studies (Baldauf et al. (2008), Bowker et al. (2007), Baldauf et al. (2016), Lee et al. (2018)) have shown that, with the exception of a few wind conditions, a NB has a positive impact in reducing downstream pollutant concentrations. Schulte et al. (2014) attribute the positive influence of the NB not only to the lifting of the emissions induced by the NB, but also to the additional turbulence around it, leading to better mixing of the pollutants. These conclusions have been reinforced by similar results observed in laboratory-scale measurements (Heist et al. (2009), Steffens et al. (2014), Pournazeri & Princevac (2015)) as well as numerical simulations (Hagler et al. (2011), Steffens et al. (2013), Schulte et al. (2014)).

There are several factors influencing the pollution dispersion around a NB (for example, atmospheric stability and roadway configuration). The topography upstream of the NB is expected to be critical as well. Street canyons display several different flow regimes depending on the geometry of the canyon, which subsequently affects the pollutant dispersion from the highway. The three flow regimes demarcated by Oke (1988) are: the isolated roughness flow regime, the wake interference regime and the skimming flow regime. These were shown to be strongly dependent on the canyon aspect ratio (AR_{canyon}) i.e. the ratio between canyon width (w_{canyon}) and canyon height (h_{canyon}). Similarly, a highway canyon can be formed via two NBs (in place of two buildings which form a street canyon). Ahangar et al. (2017) showed that an additional upwind NB further enhances the impact of the downstream NB.

NBs are capable of dispersing the air pollutants, leading to significant reductions in peak concentrations of harmful substances. However, they do not eliminate the pollutants. One possible solution is the installation of artificial semi-permeable pollutant sinks on top of these NBs, which can capture or treat the pollutants. These are permeable enough to allow for the passage of the polluted air, but not too permeable to let the pollutants pass through uncollected. One such example is the 'Open Air Line ESP' (Antea group Nederland (2016), Alfonsi et al. (2013)). The acronym ESP stands for Electrostatic Precipitator. Corona discharge from high voltage wires charges the incoming particulate matter, which then settle onto the grounded plates, after being driven by the internal electrostatic fields. There are two associated efficiencies with such a device: (i) the collection efficiency ($\eta_{\text{collection}}$), given by the mass of particles captured ($\dot{m}_{\text{collected}}$) as a percentage of the mass entering ($\dot{m}_{\text{sink}}$), and (ii) the aerodynamic efficiency ($\eta_{\text{aerodynamic}}$), defined as the mass of pollutants reaching the inlet ($\dot{m}_{\text{sink}}$) as compared to the mass emitted at the highway ($\dot{m}_{\text{emitted}}$). To this end, the overall efficiency (η_{total}) can be described by:

$$\eta_{\text{total}} = \eta_{\text{collection}} \cdot \eta_{\text{aerodynamic}} = \frac{\dot{m}_{\text{collected}}}{\dot{m}_{\text{sink}}} \cdot \frac{\dot{m}_{\text{sink}}}{\dot{m}_{\text{emitted}}} \quad (1)$$

Information about the collection efficiency can be obtained through tests under controlled environments. However, quantifying the aerodynamic efficiency is a more complicated task, which is the focus of the current study. In the remainder of the article, the aerodynamic efficiency shall be denoted simply by η.

An analogy between the semi-permeable artificial pollutant sinks and vegetation can be drawn. These too not only affect the aerodynamics of the emissions dispersion, but also remove the pollutants (Janhäll (2015)). Vegetation can be employed independently to create a porous barrier, or can also be used in tandem with NBs. Most studies on the influence of vegetation on air quality are either field studies or numerical simulations, owing to the complexity in maintaining the similarity criteria for the

vegetation. Scaling down of vegetation for laboratory-scale experiments involves maintaining similar permeability, which here is fulfilled via the pressure loss coefficient (Gromke (2011)). A summary of factors affecting the effectiveness of roadside vegetative barriers is given by Baldauf (2017).

There are fewer studies which look into the combined effect of a NB and vegetation. Field studies (Bowker et al. (2007), Baldauf et al. (2008), Lee et al. (2018)) show that the addition of vegetation enhances the removal of ultrafine particle concentrations away from a highway. This combination is often formed by having a taller vegetation barrier behind (opposite side from the road) a NB. 'Green walls' (climbing vegetation growing on the NB surface) may improve the local air quality (Pugh et al. (2012)). The geometry with vegetation and a solid surface, most closely resembling the configuration studied here, is a 'green roof' (Baik et al. (2012)), which too may improve local air quality under certain wind conditions.

While the impact of NBs on air pollution dispersion has been studied in depth, the effect of adding a semi-permeable 'pollutant sink' on top remains unclear. The only existing directly related study, to the best of the authors' knowledge, is Alfonsi et al. (2013), where the aerodynamics of the pollutant sink was studied in a simplified manner via flow visualization experiments. Large-eddy simulations were performed too, but it was assumed that the pollutant sink did not affect the flow. Nevertheless, these studies provided initial hints on the optimal placement of the pollutant sinks. In addition, there are no studies with vegetation installed in this configuration (i.e. growing on top of NBs). Thus, before the large-scale installation of pollutant sinks along kilometres of highways, it is imperative that a controlled, quantitative study be performed to obtain better and more realistic ballpark estimates about the aerodynamic performance of the pollutant sinks.

This experimental study aims to understand the aerodynamic impact of installing a pollutant sink on top of a NB located adjacent to a highway at a rural-urban fringe. The problem statement is also illustrated in Figure 1, where the NB and the sink are submerged in a turbulent Atmospheric Boundary Layer (ABL). More specifically, it is desired to reveal the configurations under which the pollutant sink performs most favourably. Here, the aerodynamic performance of the sink is defined as the percentage of the emitted highway pollution that is convected through the device (Equation (1)). Simultaneous planar Particle Image Velocimetry (PIV) and planar Laser Induced Fluorescence (LIF) measurements have been performed and the results near the NB are used to quantify the aerodynamic performance. The parameters considered are restricted to the NB height, vertical displacement of the sink with respect to the NB and different aspect ratios of highway canyons. The favourable configurations can then be used as initial guidelines for the installation of pollutant sinks near highways, in order to make the most of the investment.

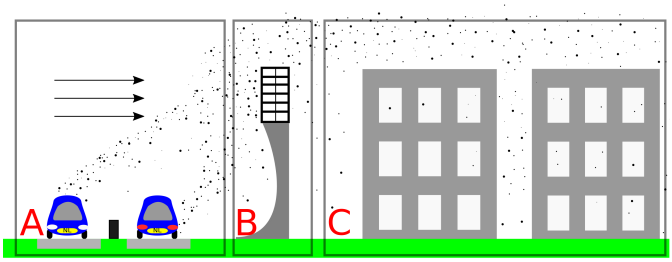

Figure 1: A schematic demonstrating the problem statement simulated via scaled down experiments. Shown here is the phenomenon of air pollutant dispersion at a typical rural-urban transition. The wind is blowing from left to right. Regions A and C correspond to the highway and the downstream urban area, respectively. Region B has a NB with a semi-permeable pollutant sink on top, which can either capture or treat certain pollutants. Objects are not drawn to scale.

The remainder of the article is structured as follows. The techniques involved in setting up the experiments as well as the definition of 'Aerodynamic efficiency' of the sink are put forth in Section 2. This is followed by Section 3, where the effect of the aforementioned parameters on the

aerodynamic performance of the sink are shown. Furthermore, the interpretation of the results from the simplified model are put in perspective with respect to the real atmospheric conditions. Finally, the major findings of this study along with possible future directions are summarized in Section 4.

2. Experimental procedure

2.1. Components of the setup

The experiments were performed in a horizontal, recirculating, closed-loop water tunnel located at the Laboratory for Aero- and Hydrodynamics, in the Delft University of Technology. The inlet is preceded by a set of flow straighteners with the flow turbulence intensities at the inlet being less than 1%. The water tunnel has a width of approximately 60.0 cm, while the water level, with the tunnel dormant, was maintained at approximately 63 cm from the bottom of the water channel, for all the experiments. The side walls of the water tunnel are built from plexiglass allowing for optical access.

The experimental setup utilized is illustrated in Figure 2. The different components are assessed below. A false floor with dimensions 450 $\times$ 60 cm^2 was mounted 17 cm above the bottom of the water channel. Being closer to the centerplane of the contraction outlet, the incoming flow on the false floor is expected to have fewer inhomogeneities. It also allows for the installation of the line source. Triangular spires were installed 42 cm downstream of the sharp leading edge of the false bottom while an additional barrier with a height of 2 cm was placed approximately 12 cm upstream of the spires. This combination led to the development of an ABL in the water channel. Further details of the triangular spires can be found in Eisma (2017). The spanwise layout of the spires was 6.5-12.5-18.5-11.5-11, with the first and last numbers representing the distance between a spire and the adjacent side wall, in cm. While not studied here, a spanwise inhomogeneity in the mean velocity of 7.5% exists for a slightly different layout of spires: 10.5-11-17-11-10.5 (Eisma (2017)). The design for the spires is inspired by the work of Irwin (1981).

The neutrally stratified ABL was characterized 340 cm downstream of the spires, at a mean freestream velocity (U_∞) of 0.74 m/s. For a flow without spires, an acceleration parameter of 2 $\times$ 10^{-8} was reported (Eisma (2017)). The mean velocity profile (u) along the wall-normal direction (z) in both, outer and inner scaling, as well as the root mean square velocity fluctuation profiles (u', w') along the wall-normal direction are summarized in Figure 2. This data has been obtained by considering velocity vectors, measured using PIV, over a streamwise length of 16.8 cm. An ABL with a height (δ_{99}) of nearly 30 cm is attained. From the inner scaling, a good agreement with log-law fit of Karman is observed between the wall-normal coordinates of 300 and 3000 in inner scaling. The average ratio between the wall-normal and streamwise velocity fluctuations (w'and u' respectively), over the entire height is 0.60, while a value of 0.52 is expected theoretically near the ground (Teunissen (1970)). Similarly, fluctuation intensities of approximately 6.5% and 3% are obtained near the ground (floor), for the streamwise and wall-normal velocity components respectively, which is lesser than the expected values of 8.5% and 4.4%. It was seen that the measured turbulence intensities in the current study were suppressed with respect to a canonical boundary layer by approximately 20% (Alfredsson & Örlü (2010)). These deficits and inaccuracies may be attributed to the low spatial resolution (2.4 mm separation between the velocity vectors) of the PIV measurements (Lavoie et al. (2007)).

Scaled down experiments to study atmospheric pollution dispersion have been employed for several decades and similarity satisfaction criteria have already been summarized in depth (Snyder (1972), Meroney (2004), Tominaga & Stathopoulos (2016)). A relevant dimensionless number for pollution dispersion experiments is the Reynolds number (based on surface-mounted obstacle height and

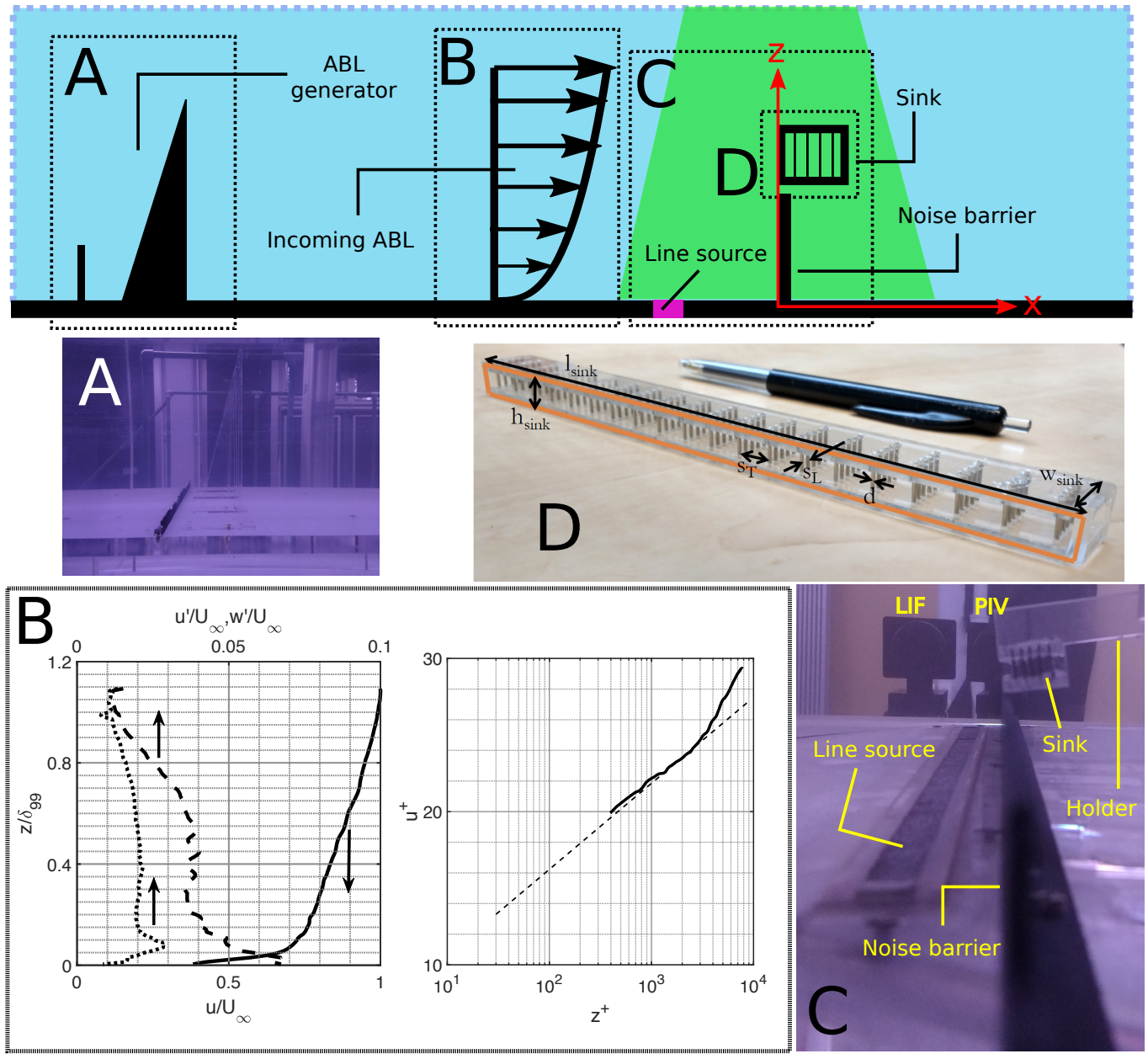

Figure 2: A schematic of the experimental setup along with (photo)graphs of the actual components (labelled A-E). Objects are not drawn to scale. The convention for the coordinate axes (x and z) is shown as well. A - The barrier and triangular spires used to simulate the ABL. B - Characteristics of the simulated ABL in, both, outer and inner scaling (placed on the left and right respectively). In the outer scaling, ——, - - and ····· represent the streamwise mean, streamwise fluctuating and wall-normal fluctuating velocity components respectively. In the inner scaling, —— and - - represent the current data and the log-law fit respectively. The superscript $^+$ refers to the inner scaling. C - The test section illuminated by the thin laser sheet consisting of the line source (in pink), the NB and the pollutant sink. These are mounted on the ground or the false floor. The holder which connects the sink to a traverse mechanism is located 5 cm behind the measurement plane, thus minimizing its influence. Two cameras, one for measuring velocities and the other for measuring scalar concentrations, are used. D - A closer look at the structure of the pollutant sink model, the dimensions of which are summarized in Table 1. The surface highlighted in orange faces the incoming flow.

freestream velocity). Based on the findings of Castro (1979), this number should exceed 5000 in order to ensure the presence of a Reynolds number independent flow regime, which is satisfied in the current experiments. Since

most atmospheric flows are aerodynamically rough, it is also ensured that the Reynolds number based on the friction velocity and roughness length exceeds 2.5 (Snyder (1972)). The model NBs used are L-shaped aluminium bars, which are installed approximately 350 cm downstream of the inlet. It was desired that the models for the NB and the sink were always submerged under 40% of the ABL height, owing to the intermittent nature of the turbulent ABL. This criterion has also been recently used by Karra et al. (2017). Thus, NB heights (h_{NB}) of 10, 20, 30, 35 and 50 mm are selected. The models used in the current experiments are largely based on those used in Eisma (2017). An effort is made to create a near two-dimensional flow, i.e. trying to minimize spanwise inhomogeneities, by having the model NBs span the entire width of the water channel.

The highway emissions are modelled by a line source located 21 mm upstream of the NB. The source consists of a porous metal plate with dimensions 10 × 400 mm^2 ($L_{\mathrm{x}} \times L_{\mathrm{y}}$) located on top of a small settling chamber with cross-sectional dimensions 10 × 20 mm^2 ($L_{\mathrm{x}} \times L_{\mathrm{z}}$). Dye is injected at nine discrete points below the porous plate via hoses of equal length connected to a 4-axle syringe pump system (neMESYS, Cetoni GmbH). This ensures a homogeneous pressure distribution below the porous plate and aids the uniform injection of dye. Furthermore, the settling chamber is filled with kitchen sponge to break up the jets at each of the nine discrete injection points and homogenize the output profile. The source is submerged in the false floor such that the porous top surface of the source is flush with the floor. A dilute solution (20 mg/L) of a fluorescent dye is diffused into the flow through the porous top surface of the source at a constant volumetric flow rate of 4.5 mL/s. This corresponds to a vertical injection velocity of 1.1 mm/s or 0.15% of the freestream velocity. It is essential that the above velocity be as low as possible, as vehicular emissions are directed predominantly horizontally. For modeling purposes, Isyumov & Ramsay (1995) state that the source strength can be exaggerated without altering the flow environment or the mixing process. While the NB spans the entire width of the water channel, it is not the case with the line source. However, the release of dye from the line source was found to be uniform near the centerline of the water channel, by visual inspection (Eisma (2017)). Further details of the line source can be found in Eisma (2017) and Tomas et al. (2017).

The model for the pollutant sink was inspired by the product 'Open Air Line ESP', whose working has been summarized by the creators (Antea group Nederland (2016)). Basically, the sink model is a duct with vertical wires mimicking the internal structure of an ESP. The external and internal dimensions of the model pollutant sink are determined in a manner, so that the pressure loss coefficient of the model sink is of similar order of magnitude as that of the real ESP. The drag coefficient was estimated experimentally by making velocity measurements using a pitot-static tube, upstream and downstream of the sink model. This approach is similar to that employed by Gromke (2011) for modelling vegetation. The sink model showed a drag coefficient of approximately 0.24 at a Reynolds number (based on freestream velocity and sink height in water) of 9200, which is close to the estimated value for the device prototype (≈ 1 m high) exposed to a mean wind speed of 3 m/s. The model sink was suspended on top of the NB, with its centerline in line with the centerline of the water channel, using a traverse mechanism which allowed for translation in the vertical (wall-normal) direction. A holder connects the traverse mechanism to the sink. It is desired that the traverse mechanism and the holder have minimal interference on the flow entering the sink. To that end, the holder is located 5 cm away from the centerline of the model sink (i.e. 5 cm behind the measurement plane) while the traverse mechanism is located 6 cm downstream of the trailing edge of the sink. The dimensions of the model sink are also summarized in

Table 1.

Table 1: Dimensions of the model sink in mm. l_{sink}, w_{sink} and h_{sink} are the length, width and height respectively. d, s_{T} and s_{L} are the wire diameter, transverse pitch of the wire mesh and longitudinal pitch of the wire mesh respectively.

l_{sink}	w_{sink}	h_{sink}	d	s_{T}	s_{L}
200.0	17.54	11.71	1	10	2.5

Simultaneous planar PIV and planar LIF was employed in the current measurements, to obtain fluid velocities and dye concentrations in the mid-plane of the tunnel containing the streamwise and wall-normal directions. The field of view (approximately 15×10 cm^2) was illuminated by a twin-cavity double pulsed Nd:YAG laser (Spectra-Physics Quanta Ray). For PIV, the flow was seeded with 10 μm Sphericell tracer particles. Images were captured by a Flowmaster Imager Intense camera with a digital resolution of 1376×1040 pixels, which was equipped with a Nikkor f35 mm lens (at an aperture number of 5.6) as well as a 550 nm shortpass green color filter (to minimize the contamination by the signal from the fluorescent dye). A second combination of the same camera and lens (also maintained at an aperture number of 5.6, albeit with a 590 nm longpass red color filter in front) was used for the planar LIF experiments. Rhodamine WT was used as the fluorescent dye to simulate the passive scalar (i.e. pollutants). This dye has an absorption peak at 558 nm and emission peak at 582 nm (Wilson et al. (1986)). While the PIV camera looked straight at the region of interest, the LIF camera was at a small angle of approximately 5° with respect to the measurement plane normal. In addition, both the cameras had a slight vertical inclination. All images were acquired and processed using the commercial software DaVis 8.4.0. The PIV images were further processed using a multi-pass interrogation technique, where the final windows had a size of 16×16 pixels, with 50% overlap between the neighbouring windows. No calibration was performed for the planar LIF experiments, i.e. greyscale intensities of the dye (I) were not converted to a concentration value. However, as will be shown later, this is not expected to influence the quantities of interest. Furthermore, no image dewarping operation was performed on the planar LIF images as the viewing angle of the camera was small. While the fluorescent dye intensity was available at a spacing corresponding to nearly 0.1 mm, the velocity vector spacing was approximately 0.8 mm (corresponding to nearly $60 l_\eta$, where l_η is an estimate for the Kolmogorov scale). Image pairs were taken every 0.2 s (more than twice the estimated integral time scale), i.e. consecutive velocity-scalar fields were statistically uncorrelated. Each experiment consisted of 150 flow fields. Further data processing was performed using Matlab R2017a, where information from the coarser PIV grid was interpolated onto the finer LIF grid using the cubic spline method. Background images were also captured before and after each set of experiments, which allowed for the correction of the accumulation of dye in the background of the water channel, via background subtraction.

2.2. Aerodynamic efficiency evaluation

A quantity of interest for the current study is the aerodynamic efficiency of the sink (η). The aerodynamic efficiency is defined as the concentration flux entering the pollutant sink, i.e. the scalar flux through the surface A in Figure 3, relative to that leaving the entire cross-section above the NB. The latter corresponds to the scalar flux through the surface B in Figure 3, which includes surface A and, on average, is equal to the emission rate from the source. Surface A is fixed to the sink (i.e. it moves up if the sink moves up), while B always spans from the NB top to the upper bound of the field of view. The aerodynamic efficiency can be expressed mathematically as:

$$\eta = \frac{\int_0^T \int_A cu \, dz \, dt}{\int_0^T \int_B cu \, dz \, dt} \approx \frac{\int_0^T \int_A \beta I u \, dz \, dt}{\int_0^T \int_B \beta I u \, dz \, dt} = \frac{\int_0^T \int_A I u \, dz \, dt}{\int_0^T \int_B I u \, dz \, dt} \tag{2}$$

where c is the scalar concentration, u is the horizontal velocity component (normal to the surfaces A and B), and β is a calibration coefficient assuming a linear relation between the scalar concentration and the dye intensity (after background subtraction). Furthermore, β is assumed constant. T is the total duration of the experiment.

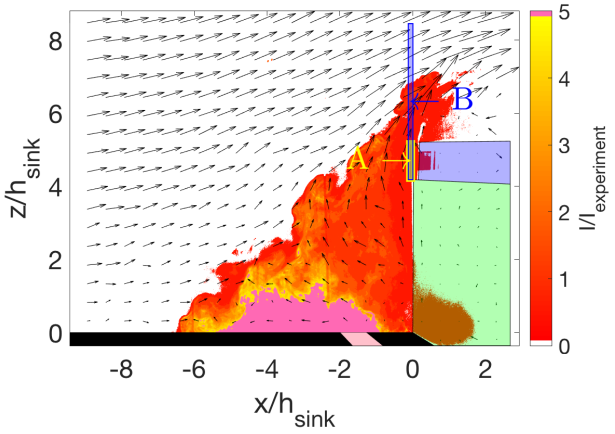

Figure 3: Definition of the aerodynamic efficiency of the pollutant sink. Shown in this figure are the instantaneous velocity vectors as well as contours of the normalized instantaneous dye intensity. Intensities are normalized by $I_{\text{experiment}}$, which is the spatio-temporal mean intensity from a single experiment. Only every sixth vector in each direction is shown for clarity. The ground is depicted in black with the location of the embedded line source in pink. The area in light green is the NB while the area in light blue is the pollutant sink. Velocity vectors in the light green and light blue patches are the vectors corresponding to those downstream of the NB and the pollutant sink respectively. Shown also are the rectangular areas, A and B (in yellow and blue respectively), used to evaluate the aerodynamic efficiency.

Calibration curves from the study of Eisma (2017), using a similar setup, indicate that calibration coefficients in regions of homogeneous laser intensity are indeed nearly identical. Furthermore, a linear behaviour between fluorescence intensity and concentration has been seen for Rhodamine WT (Alméras et al. (2016)) for concentrations up to 50 mg/L. Another concern in planar LIF measurements, that was first introduced and quantified by Vanderwel & Tavoularis (2014), is the presence of secondary fluorescence (fluorescing of out-of-plane dye excited by light emitted by in-plane fluoresced dye). It has been shown that secondary fluorescence may contribute up to 50% of the total signal. Baj et al. (2016) have proposed a calibration procedure which allows the local amount of secondary fluorescence to be determined. Their results indicate that the percentage contribution of secondary fluorescence to the total fluorescence does not vary strongly in space. This would mean that secondary fluorescence would not significantly affect the aerodynamic efficiency, which is based on relative concentration values (Equation (2)).

Thus, the second equality in Equation (2) may also be utilized as an accurate measure of the aerodynamic efficiency. The quantity 'Iu' (product of dye intensity and streamwise velocity at a given location) is referred to as the intensity based flux hereafter.

3. Results

Three different sets of experiments were performed, schematics of which are drawn in Figure 4. The three parameters are: the height of the NB, the vertical position of the sink with respect to the NB, and the aspect ratio of the highway canyon (formed by using an additional NB).

3.1. A pollutant sink performs better on a shorter noise barrier

The first case to be investigated was the flow of pollutants towards a NB with the sink mounted flush on top of it, as illustrated in Figure 4(a). Five different NB heights were considered, with the ratio between the NB height and the sink height varied from 0.85 to 4.27.

The average flow for the cases of the two extremities of the NB heights are shown in Figure 5(a)-(b). While qualitative, the time-averaged velocity vectors and normalized dye intensity patterns already indicate that a sink on top of a shorter NB is expected to perform better aerodynamically. The flow for the taller fence consists of a rather large upstream separation bubble, causing the incoming flow to separate at a steeper angle, with respect to the bottom

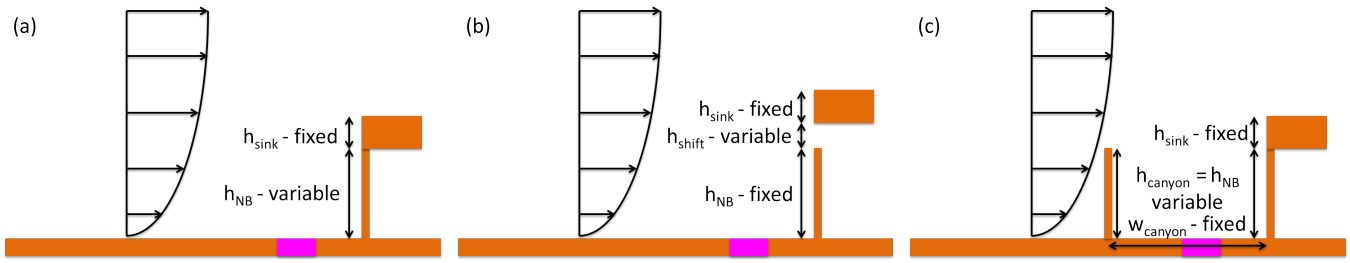

Figure 4: Schematics of the different cases considered in this study. A pollutant sink of fixed dimensions installed on (a) NBs of varying heights (b) A NB of fixed height but varying vertical elevations of the sink (c) Highway canyons with varying aspect ratios.

surface, which leads not only to a higher angle of the flow in front of the sink, but also a larger vertical dispersion of the dye. This is in line with the expectation that taller NBs increase the dispersion of pollutants in the vertical direction (Schulte et al. (2014), Pournazeri & Princevac (2015)).

The above trend is also quantified in Figure 5(c) with the aerodynamic efficiency of the sink decreasing with increasing NB heights. This is attributed to the lower magnitudes of the horizontal velocity component caused by the higher flow angles as shown in Figure 5(d)-(e). These higher flow angles also contribute to a higher vertical spread of the dye, i.e. lower dye concentration at the entrance of the sink, leading to a drop in the aerodynamic efficiencies. In these plots, the horizontal velocity component is normalized by the maximum horizontal velocity component ($u_{\max}$) in the cross-section above the NB (i.e. Region B in Figure 3) which can vary up to 5% for a set of experiments where only a single parameter is being investigated. It should be noted that results for the cases with $h_{\mathrm{NB}} = 2.56h_{\mathrm{sink}}$ and $h_{\mathrm{NB}} = 4.27h_{\mathrm{sink}}$ are ensemble averages of five experimental runs, while the remaining are results from a single experiment.

Earlier work attempted to estimate the aerodynamic efficiency of a sink without an actual sink device (resistance) present in the flow (for example, the numerical simulations of Alfonsi et al. (2013)). Experiments here demonstrate that even though such an approach reveals a similar trend, the efficiency can be overestimated by up to 10%. This inference was made by recreating the experiments without the presence of the sink and assuming an imaginary sink present on top of the NB when evaluating the aerodynamic efficiency using Equation (2). However, the addition of a semi-permeable sink, creates a de facto taller NB leading to lower horizontal velocity magnitudes and slightly higher flow angles. While the overall trends are not very different, the quantities are. Thus, it is recommended that experiments include a sink, since it affects the upstream flow.

3.2. Slightly raising the pollutant sink enhances its aerodynamic performance

Intensity based flux profiles in region B (the region is shown in Figure 3) from the experiments in Section 3.1 suggested that raising the sink may enhance its aerodynamic performance. This led to the next set of experiments, whose schematic is illustrated in Figure 4(b). The sink was shifted vertically with respect to the NB for two different NB heights ($h_{\mathrm{NB}} = 2.56h_{\mathrm{sink}}$ and $h_{\mathrm{NB}} = 4.27h_{\mathrm{sink}}$). It should be noted that the cases with $h_{\mathrm{shift}} = 0$ correspond to results from Section 3.1.

Two cases of raising the sink for a NB with $h_{\mathrm{NB}} = 4.27h_{\mathrm{sink}}$ are illustrated in Figure 6(a)-(b). When the sink is raised only slightly ($h_{\mathrm{shift}} = 0.10h_{\mathrm{NB}}$), as in Figure 6(a), a small gap is formed which is not large enough to let a lot of dye to escape. Thus, sufficient quantities of dye still reach the sink inlet. However, it cannot be concluded yet whether this elevation aids or afflicts the flow of the pollutants towards the sink, as compared to the case with

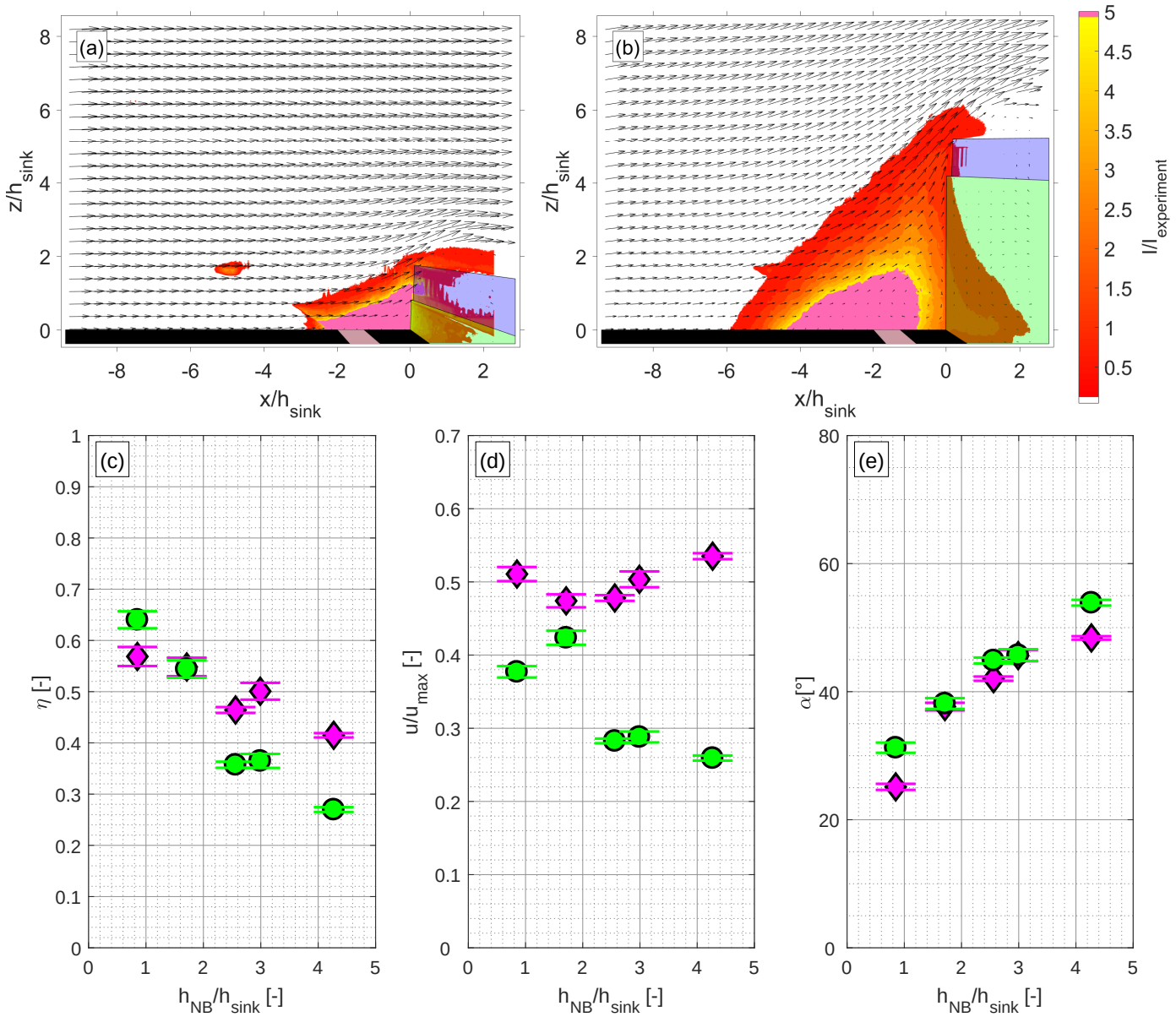

Figure 5: Installing a pollutant sink is more effective on shorter NBs. A sink on a shorter NB is exposed to an incoming flow at a smaller angle with respect to the horizontal, owing to the smaller mean upstream separation bubble which also leads to a smaller vertical dispersion of the dye. Contours of the time-averaged normalized mean dye intensity and mean velocity vectors are shown for (a) $h_{\mathrm{NB}} = 0.85\ h_{\mathrm{sink}}$ (b) $h_{\mathrm{NB}} = 4.27\ h_{\mathrm{sink}}$. The effect of NB height on (c) Aerodynamic efficiency of the sink, (d) Horizontal velocity component at the inlet, (e) Angle of flow (α) at the inlet, are quantified. ● and ◆ in (c), (d) and (e) mark the mean values, for the respective plot, with and without a sink, while the vertical error bars represent the standard error on the mean. The case with a sink has the model sink present in the flow whereas the case without a sink does not have one. The quantities for the latter are thus computed assuming the presence of a hypothetical sink. The mismatch of results between the two cases imply that without an actual sink, inaccurate predictions of the aerodynamic efficiency may be made.

no sink elevation. The other extreme where the sink is displaced by a large distance ($h_{\mathrm{shift}} = 0.40 h_{\mathrm{NB}}$), like in Figure 6(b), indicates that the gap formed here, in between the sink and the NB top, allows a rather generous amount of dye to pass, which is undesirable.

The aerodynamic efficiency trends in Figure 6(c) highlight that slightly elevating the sink is beneficial in enhancing its aerodynamic performance (a near 10% enhance-

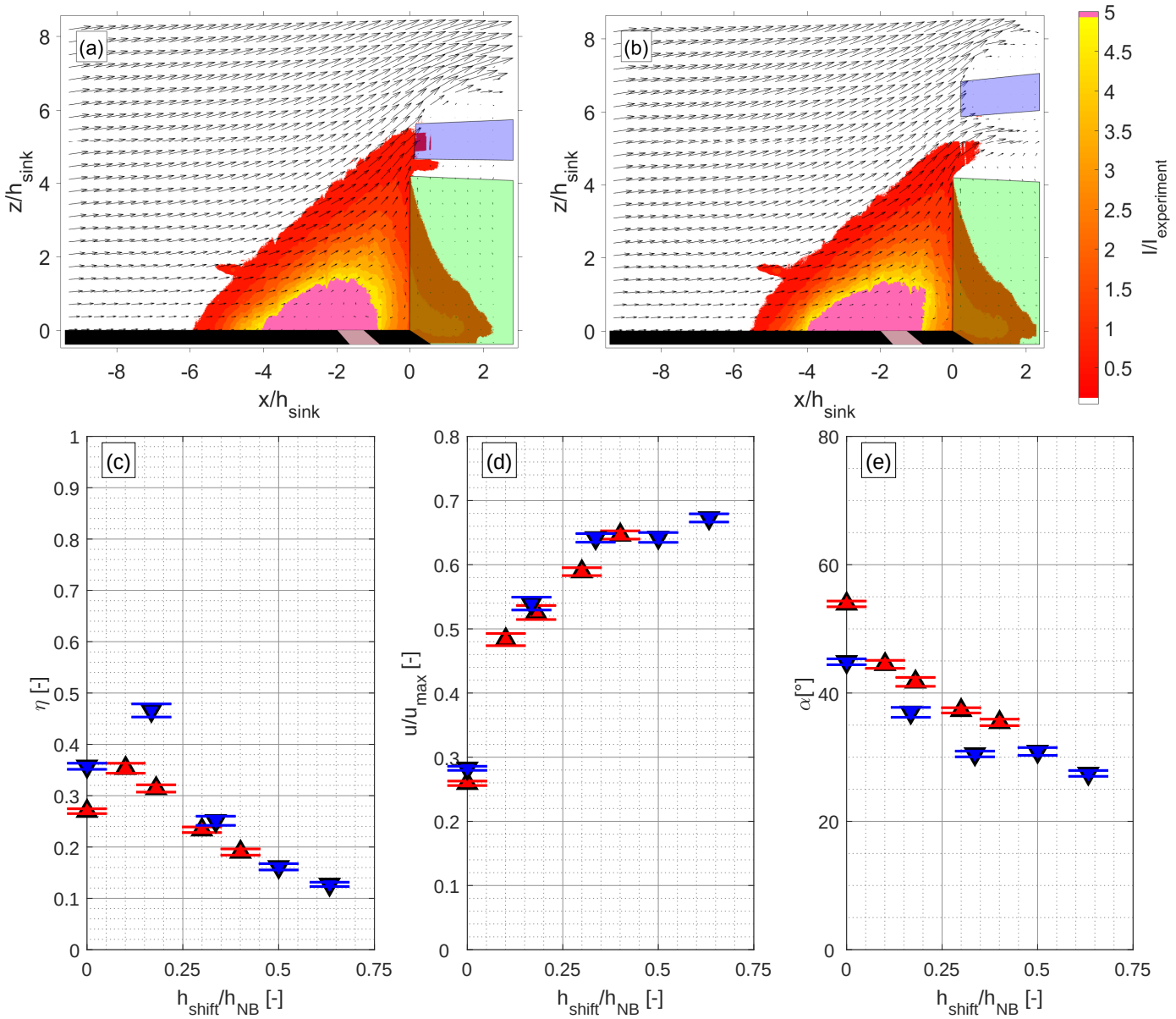

Figure 6: Slightly raising the pollutant sink enhances its effectiveness. A twofold increase in the horizontal velocity component aided by a near 10° decrease in the flow angle is a major contributor to this enhancement. Raising the sink too much creates a huge gap between the NB and the sink allowing a generous amount of dye to escape. Contours and vectors present, respectively, the time-averaged normalized mean dye intensity and the mean velocity vectors for $h_{\mathrm{NB}} = 4.27\ h_{\mathrm{sink}}$ and (a) $h_{\mathrm{shift}} = 0.10\ h_{\mathrm{NB}}$ (b) $h_{\mathrm{shift}} = 0.40\ h_{\mathrm{NB}}$. The vertical elevation of the sink is shown to affect the (c) Aerodynamic efficiency of the sink, (d) Horizontal velocity component at the inlet, (e) Angle of flow (α) at the inlet. ▲ and ▼ in (c), (d) and (e) are the mean values for the respective plot for $h_{\mathrm{NB}} = 4.27\ h_{\mathrm{sink}}$ and $h_{\mathrm{NB}} = 2.56\ h_{\mathrm{sink}}$, respectively, while the vertical error bars represent the standard error on the mean.

ment). This is explained by the near twofold rise in the magnitude of the horizontal velocity component just upstream of the sink, aided by a 10° drop in the flow angle (which contributes a factor of 1.4 increase in the horizontal velocity component) as illustrated in Figure 6(d)-(e). The remaining increase in the horizontal velocity upstream of the sink may be attributed to elevating the sink in the ABL, whereby it is placed in a region with a higher horizontal velocity. Further raising the sink causes the horizontal velocity to increase even more. However, the

dye concentration decreases, which again reduces the efficiency, leading to an optimum elevation. A similar set of experiments were also performed with a NB with $h_{\mathrm{NB}} = 2.56h_{\mathrm{sink}}$, and the results confirm that a slight vertical elevation of the sink is beneficial for its aerodynamic performance.

3.3. Installing a pollutant sink in a canyon must be done with care

The findings of Oke (1988) on the sensitivity of flow regimes to street canyon aspect ratios led to the next set of experiments. A 'highway canyon' was formed by adding a NB upstream of the line source in a manner that the line source was placed exactly in between the two NBs.

A major difference between the typical 'street canyon' often formed by cubical blocks and the 'highway canyon', illustrated in Figure 4(c), is that the upstream NB here is the first roughness element encountered by the flow. Typical studies of street canyons immersed in an ABL include several upstream roughness elements over which the flow develops. In addition, the roughness elements here are much thinner.

The dispersion of the dye for four different canyon aspect ratios is illustrated in Figure 7(a),(c)-(e). All four cases have in common, a shear layer detaching from the top of the upstream NB and reattaching downstream. The downstream distance of the reattachment point is expected to be proportional to the NB height. The first case considered is the canyon with the lowest aspect ratio ($AR_{\mathrm{canyon}} = 0.84$). It is expected that for such a low aspect ratio canyon, the reattachment point of the separated shear layer lies further downstream of the downstream NB (outside of the field of view). For the low aspect ratio canyon, the downstream NB lies in this region of reverse flow associated with the flow separated from the upstream NB. The reverse flow in the wake of the upstream NB approaches the downstream NB and re-enters the highway canyon via the semi-permeable pollutant sink. This reverse flow through the pollutant sink induces a weak counterclockwise circulation region in the canyon. When the dye is released from the line source, it would follow the recirculation in the canyon, and is driven away from the sink by the reverse flow through and over the sink. Under such conditions, the pollutant sink is expected to be useless. To solve this problem, an experiment with the sink raised above the detached shear layer ($h_{\mathrm{shift}} = 0.30h_{\mathrm{NB}}$) was performed. No major changes in the flow regime were observed, as can be seen in Figure 7(b), with the exception of a relatively stronger counterclockwise circulation region in the canyon. This may be attributed to a negative wall-normal velocity component near the gap formed between the sink and the NB top. In this case, a larger amount of the dye reaches the sink inlet, and thus, elevating the sink is advisable under such canyon configurations. A canyon with a slightly higher aspect ratio ($AR_{\mathrm{canyon}} = 1.41$) did not show any change in the flow regime, with backward flow through the sink, a weak counterclockwise flow in the canyon and the dye escaping the canyon over the sink. In this canyon too, raising the sink by an appropriate amount, so as to intercept the shear layer, would be beneficial.

On the other end of the spectrum, for the canyon with the highest aspect ratio ($AR_{\mathrm{canyon}} = 4.17$), the shear layer detaching from the upstream NB does not pass over the top of the downstream NB, and two circulating regions are formed: A strong clockwise circulation region just upstream of the downstream NB, which drives the dye towards the sink entrance and a weak counterclockwise circulation just downstream of the upstream NB, which has a negative effect in driving the dye out of the canyon. Thus, in this case, the sink is effective as opposed to the canyons with low aspect ratios.

The last case considered was that of a canyon with an intermediate aspect ratio ($AR_{\mathrm{canyon}} = 2.08$). The detached shear layer here is intercepted by the sink, which also induces a single, strong clockwise circulation region which drives a large amount of dye into the sink. However, an

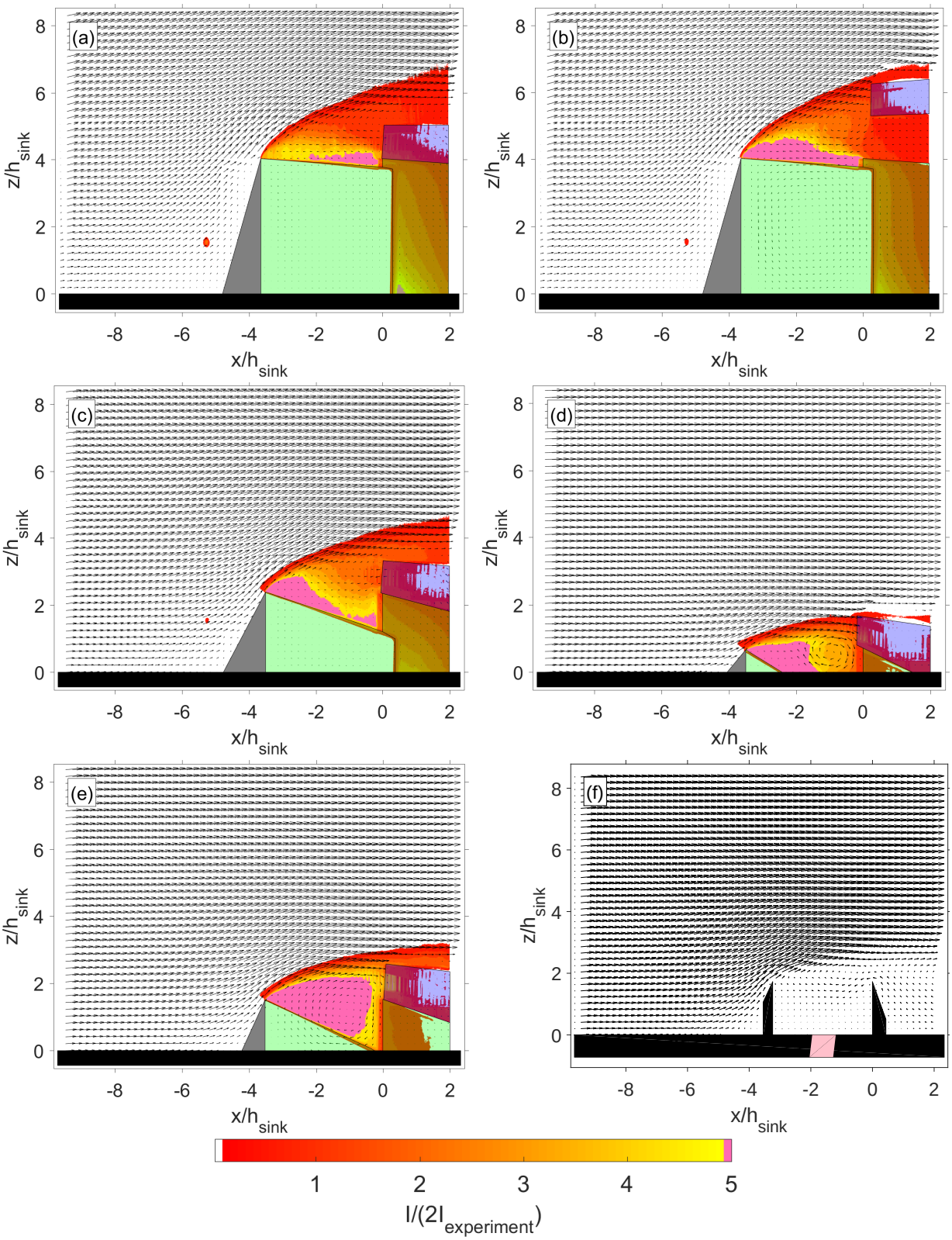

Figure 7: The flow regime in an isolated highway canyon is dependent on the canyon geometry. Contours of the time-averaged normalized mean dye intensity and mean velocity vectors are shown for cases with a pollutant sink installed in canyon with (a) $AR_{\text{canyon}} = 0.84$ (b) $AR_{\text{canyon}} = 0.84$ and $h_{\text{shift}} = 0.3h_{\text{NB}}$ (c) $AR_{\text{canyon}} = 1.41$ (d) $AR_{\text{canyon}} = 4.17$ (e) $AR_{\text{canyon}} = 2.08$. (f) Velocity vectors when the sink is removed from the canyon with $AR_{\text{canyon}} = 2.08$.

experiment for the same canyon geometry minus the sink, illustrated in Figure 7(f), showed that the region immediately above the downstream NB has reverse flow. This means that flow regime changes in the canyon can not only brought up by the change in the canyon aspect ratio, but also by the addition/removal of a sink.

3.4. Caveats

The experiments performed, and hence the results obtained, pertain to a very simplistic geometry. Pollutant sinks are eventually meant to be installed along real highways, and reality offers a lot more complications as compared to the simplified model considered here. The uncertainties surrounding the experiment as well as the non ideal scenarios existing by real highways are discussed below.

In the current experiments, the geometry was two-dimensional such that the velocity and scalar statistics are homogeneous along the NB, as would approximately be the case along extended stretches of a highway. However, actual NB geometries can be three-dimensional. Numerical simulations (Steffens et al. (2013), Hagler et al. (2011)), laboratory measurements (Steffens et al. (2014)) as well as field measurements (Baldauf et al. (2008)) have noted the presence of an edge effect where the flow (i.e. the pollutants) meanders about the edge, which would afflict the aerodynamic efficiency of the sink. Another major simplification in the current study is the cross-wind situation, with the wind being perpendicular to the highway.

The fluorescent dye used in the experiments simulates the flow of an inert pollutant which follows the fluid flow very accurately. However, as introduced earlier, there exists a variation in the sizes of PM, each with different fluid tracing properties, which may raise the question about the applicability of the current results to actual scenarios. The Stokes number (i.e. the particle response time relative to the time scale of the flow) is about 0.002 for a particle with a diameter of 10 μm, density of 2600 kg/m^3 suspended in wind blowing at 10 m/s, around a 5 m tall NB. Note that the mentioned Stokes number is based on the time scale for the fluid to pass the NB, and not the kolmogorov time scale. This is justifiable because the current study is not concerned with the small-scale dynamics of the particle. Based on the small Stokes number (< 0.1), it can be said that the particle motion closely follows that of the fluid, similar to the dye. Hence, the results from the current dye experiments can be considered representative for PM_{10}. The Stokes number for $PM_{2.5}$ and $PM_{0.1}$ are even smaller such that these particles are expected to faithfully follow the small-scale motions too. Thus, the results from the current study would be equally applicable to these particles as well.

One restriction of the current experiments is the study being performed under a neutral ABL. However, it is likely that the pollutant sink would operate also under stable and unstable ABLs, which would change the results. For example, under non-neutral atmospheric conditions, the shape of turbulent eddies is elliptical, i.e. the dispersion of pollutants is expected to be anisotropic (Stull (2016)). Besides these, the ABL velocity profiles are markedly different. Under unstable conditions, the pollutants will have extra turbulent energy in the vertical direction and thus, more propensity to escape the sink, while under stable conditions, the turbulent energy in the vertical direction would be suppressed, enhancing the sinks aerodynamic performance. Similarly, semi-empirical models have demonstrated that under very stable conditions, the effect of the NB persists to larger downwind distances as compared to neutral and unstable conditions (Schulte et al. (2014)).

The source of pollutants in the current investigation is that released by vehicles, which are also the fastest moving objects on the road. While the turbulence induced by the vehicles is neglected here, under really calm conditions (on-road wind speed ≤ 1 m/s), it is expected to start playing a major role, as asserted by Eskridge & Rao (1986). Laboratory experiments demonstrated that turbulence in-

duced by two-way traffic along the highway causes additional diffusion of pollutants (Kastner-Klein et al. (2001)), which is expected to cause a drop in the aerodynamic performance of the pollutant sink. However, one way traffic is expected to drive the pollutants along the highway and not significantly affect the aerodynamic performance of the sink. Similarly, increased traffic velocity and density is expected to enhance the turbulent diffusion of the pollutants (Kastner-Klein et al. (2000)) and decrease the sink's aerodynamic performance.

The presence of vegetation around the highway too is expected to affect the pollutant dispersion - not only the aerodynamics, but also acting as a natural sink itself (Janhäll (2015), Gromke & Ruck (2007)). Depending on the size and placement of vegetation, they can either enhance or inhibit the aerodynamic performance of the sink, and their effect should be understood in a case by case basis.

In addition, the current study has disregarded the presence and influence of upstream and downstream urban areas. Upstream roughness elements would disrupt the incoming ABL and thus, the flow over the highway would be affected as well. While downstream roughness elements are not expected to influence flow near the highway much, it is possible that for the highway canyons with the low aspect ratios ($AR_{\text{canyon}} = 0.84$ and $AR_{\text{canyon}} = 1.41$), the downstream objects may affect the reattaching shear layer and the subsequent backward flow through the semi-permeable pollutant sink.

Besides the aerodynamic efficiencies, the scaled down PIV and LIF experiments are also capable of providing flow statistics at the sink inlet. Since it is possible that the collection/treatment efficiency of the sink is a function of the incoming flow velocity, the incoming flow velocity can also provide an estimate for the collection/treatment efficiency. Similarly, the flow angle can provide an indicator for the optimal placement of the sink. Aligning the inlet cross-section area of the sink perpendicular to the incoming flow is expected to enhance the aerodynamic efficiency of the sink. Nevertheless, tilting the sink can also strongly affect the pollution dispersion, based on the results of street canyon flows with varying roof shapes (Huang et al. (2009), Yassin (2011), Takano & Moonen (2013)).

Owing to these uncertainties, it is highly recommended that field tests also be employed prior to large-scale installation, in order to be fully confident about their effectiveness. Nevertheless, the scaled-down experiments from the current study already provide important indications on the optimal positioning and orientation of these sinks.

4. Conclusions

The optimal installation location of the air pollutant sinks atop NBs adjacent to highways has been looked into, via scaled down experiments. The quantity 'aerodynamic efficiency' was defined to evaluate the aerodynamic performance of the pollutant sink. The major findings of this study are summarized below:

- Installing a pollutant sink (with fixed dimensions) flush on top of a shorter NB is found to be more effective than on taller NBs. This is attributed to the presence of a rather large mean separation bubble upstream of the taller NBs, which leads to larger vertical dispersion of the dye.

- A slight vertical elevation of the sink from the top of the NB is beneficial to its aerodynamic performance. This slight elevation leads to a twofold increase in the horizontal velocity component, while the small gap between the NB and the sink only allows a small amount of the passive scalar to escape.

- The flow regimes in a highway canyon (two NBs placed in symmetrically opposite location with respect to the line source) is dependent on the canyon aspect ratio (ratio between canyon width and canyon height). For low aspect ratio canyons, backward flow

through the semi-permeable sink is observed. In such configurations, the sink effectively tackles pollutants arising downstream of the highway instead of those arising from the highway, which is undesirable. In such cases, the solution involves raising the sink to the same height as the shear layer separating from the upstream NB. For higher canyon aspect ratios, the sink is effective when installed atop the nb. It is also observed that, for certain intermediate canyon aspect ratios, the addition of a sink affects the flow regime by raising the effective height of the downstream NB. Thus, the flow regimes must be considered prior to the installation of sinks.

Furthermore, it is possible to determine the flow magnitude and angle at the inlet of the sink. For certain sinks, the incoming velocity of the pollutant is important in determining the collection efficiency (pollutant collected by the device relative to the amount of pollution entering the device).

The flow angle can give an indication for the optimal orientation of the sink inlet. By aligning the inlet with the incoming flow, the effective cross-section area of the inlet is increased, allowing for a higher passage of the pollutants.

Conflicts of interest

None

Funding

This research did not receive any specific grant from funding agencies in the public, commercial, or not-for-profit sectors.

Acknowledgements

The authors are grateful to George Bitter and Bob Smulders for providing the design of the 'Open Air Line ESP'. Furthermore, the authors thank Edwin Overmars, Jasper Ruijgrok and Jan Graafland for their support during the experiments.

References

Ahangar, F. E., Heist, D., Perry, S., & Venkatram, A. (2017). Reduction of air pollution levels downwind of a road with an upwind noise barrier. *Atmospheric Environment*, *155*, 1 – 10. doi:10.1016/j.atmosenv.2017.02.001.

Alfonsi, M., Eisma, J., Gezici, Ö., Jacobs, V., Knegjens, R., Roobol, S., Chris, S., van Son, M., & Tomas, J. (2013). The fine dust problem near urban highways - optimization of the electrostatic precipitator device. In *Proceedings Physics with Industry 2013* (pp. 3–24). URL: http://www.stw.nl/sites/stw.nl/files/Physics-with-Industry-2013-Proceedings.pdf.

Alfredsson, P. H., & Örlü, R. (2010). The diagnostic plot – a litmus test for wall bounded turbulence data. *European Journal of Mechanics - B/Fluids*, *29*, 403 – 406. doi:10.1016/j.euromechflu.2010.07.006.

Alméras, E., Plais, C., Euzenat, F., Risso, F., Roig, V., & Augier, F. (2016). Scalar mixing in bubbly flows: Experimental investigation and diffusivity modelling. *Chemical Engineering Science*, *140*, 114–122. doi:10.1016/j.ijmultiphaseflow.2016.03.011.

Anderson, J. O., Thundiyil, J. G., & Stolbach, A. (2012). Clearing the air: A review of the effects of particulate matter air pollution on human health. *Journal of Medical Toxicology*, *8*, 166–175. doi:10.1007/s13181-011-0203-1.

Antea group Nederland (2016). Revolutionary solution captures particulate matter. URL: http://www.anteagroup.nl/sites/default/files/infographic_open_air_line_esp_eng_-_def.pdf [Online; accessed 24-July-2017].

Baik, J.-J., Kwak, K.-H., Park, S.-B., & Ryu, Y.-H. (2012). Effects of building roof greening on air quality in street canyons. *Atmospheric Environment*, *61*, 48 – 55. doi:10.1016/j.atmosenv.2012.06.076.

Baj, P., Bruce, P., & Buxton, O. (2016). On a PLIF quantification methodology in a nonlinear dye response regime. *Experiments in Fluids*, *57*, 106. doi:10.1007/s00348-016-2190-0.

Baldauf, R. (2017). Roadside vegetation design characteristics that can improve local, near-road air quality. *Transportation Research Part D: Transport and Environment*, *52*, 354 – 361. doi:10.1016/j.trd.2017.03.013.

Baldauf, R., Thoma, E., Khlystov, A., Isakov, V., Bowker, G., Long, T., & Snow, R. (2008). Impacts of noise barriers on near-road air quality. *Atmospheric Environment*, *42*, 7502 – 7507. doi:10.1016/j.atmosenv.2008.05.051.

Baldauf, R. W., Isakov, V., Deshmukh, P., Venkatram, A., Yang, B., & Zhang, K. M. (2016). Influence of solid noise barriers on near-

road and on-road air quality. *Atmospheric Environment*, *129*, 265–276. doi:10.1016/j.atmosenv.2016.01.025.

Bowker, G. E., Baldauf, R., Isakov, V., Khlystov, A., & Petersen, W. (2007). The effects of roadside structures on the transport and dispersion of ultrafine particles from highways. *Atmospheric Environment*, *41*, 8128 – 8139. doi:10.1016/j.atmosenv.2007.06.064.

Brunekreef, B., & Holgate, S. T. (2002). Air pollution and health. *The Lancet*, *360*, 1233 – 1242. doi:10.1016/S0140-6736(02)11274-8.

Castro, I. P. (1979). Relaxing wakes behind surface-mounted obstacles in rough wall boundary layers. *Journal of Fluid Mechanics*, *93*, 631–659. doi:10.1017/S0022112079001968.

Eisma, H. (2017). *Pollutant dispersion in wall-bounded turbulent flows: an experimental assessment*. Ph.D. thesis. doi:10.4233/uuid:205f36da-9d4b-4c28-a326-864b27cb857d.

Eskridge, R. E., & Rao, S. T. (1986). Turbulent diffusion behind vehicles: Experimentally determined turbulence mixing parameters. *Atmospheric Environment (1967)*, *20*, 851 – 860. doi:10.1016/0004-6981(86)90269-6.

Gromke, C. (2011). A vegetation modeling concept for building and environmental aerodynamics wind tunnel tests and its application in pollutant dispersion studies. *Environmental Pollution*, *159*, 2094 – 2099. doi:10.1016/j.envpol.2010.11.012. Selected papers from the conference Urban Environmental Pollution: Overcoming Obstacles to Sustainability and Quality of Life (UEP2010), 20-23 June 2010, Boston, USA.

Gromke, C., & Ruck, B. (2007). Influence of trees on the dispersion of pollutants in an urban street canyon–Experimental investigation of the flow and concentration field. *Atmospheric Environment*, *41*, 3287 – 3302. doi:10.1016/j.atmosenv.2006.12.043.

Hagler, G. S., Tang, W., Freeman, M. J., Heist, D. K., Perry, S. G., & Vette, A. F. (2011). Model evaluation of roadside barrier impact on near-road air pollution. *Atmospheric Environment*, *45*, 2522 – 2530. doi:10.1016/j.atmosenv.2011.02.030.

Hamers, D., Nabielek, K., Piek, M., & Sorel, N. (2009). Verstedelijking in de stadsrandzone. Een verkenning van de ruimtelijke opgave (in dutch). *Den Haag, PBL Netherlands Environmental Assessment Agency*, . URL: http://www.pbl.nl/sites/default/files/cms/publicaties/verstedelijking_in_de_stadsrandzone_web.pdf.

Heist, D., Perry, S., & Brixey, L. (2009). A wind tunnel study of the effect of roadway configurations on the dispersion of traffic-related pollution. *Atmospheric Environment*, *43*, 5101 – 5111. doi:10.1016/j.atmosenv.2009.06.034.

Hooghwerff, J., Tollenaar, C., & van der Heijden, W. (2010). In-situ air quality measurements on existing and innovative noise barriers. In *Air Pollution XVIII* (pp. 129–139). WIT Press Kos, Greece. doi:10.2495/AIR100121.

Huang, Y., Hu, X., & Zeng, N. (2009). Impact of wedge-shaped roofs on airflow and pollutant dispersion inside urban street canyons. *Building and Environment*, *44*, 2335 – 2347. doi:10.1016/j.buildenv.2009.03.024.

Innovatieprogramma Luchtkwaliteit (2009). Review Scientific Board: International review of the Air Quality Innovation Programme (IPL). URL: https://www.rijksoverheid.nl/binaries/rijksoverheid/documenten/rapporten/2009/12/01/review-scientific-board-international-review-of-the-air-quality-innovation-programme-ipl/scientific-20board-20review.pdf.

Irwin, H. (1981). The design of spires for wind simulation. *Journal of Wind Engineering and Industrial Aerodynamics*, *7*, 361 – 366. doi:10.1016/0167-6105(81)90058-1.

Isyumov, N., & Ramsay, S. (1995). Physical Modelling of Atmospheric Dispersion in Complex Settings. In J. E. Cermak, A. G. Davenport, E. J. Plate, & D. X. Viegas (Eds.), *Wind Climate in Cities* (pp. 131–152). Dordrecht: Springer Netherlands. doi:10.1007/978-94-017-3686-2_7.

Janhäll, S. (2015). Review on urban vegetation and particle air pollution – Deposition and dispersion. *Atmospheric Environment*, *105*, 130 – 137. doi:10.1016/j.atmosenv.2015.01.052.

Karra, S., Malki-Epshtein, L., & Neophytou, M. K.-A. (2017). Air flow and pollution in a real, heterogeneous urban street canyon: A field and laboratory study. *Atmospheric Environment*, *165*, 370 – 384. doi:10.1016/j.atmosenv.2017.06.035.

Kastner-Klein, P., Berkowicz, R., & Plate, E. (2000). Modelling of vehicle-induced turbulence in air pollution studies for streets. *International Journal of Environment and Pollution*, *14*, 496–507. doi:10.1504/IJEP.2000.000573.

Kastner-Klein, P., Fedorovich, E., & Rotach, M. (2001). A wind tunnel study of organised and turbulent air motions in urban street canyons. *Journal of Wind Engineering and Industrial Aerodynamics*, *89*, 849 – 861. doi:10.1016/S0167-6105(01)00074-5.

Keuken, M., Moerman, M., Voogt, M., Blom, M., Weijers, E., Röckmann, T., & Dusek, U. (2013). Source contributions to $PM_{2.5}$ and PM_{10} at an urban background and a street location. *Atmospheric Environment*, *71*, 26–35. doi:10.1016/j.atmosenv.2013.01.032.

Lavoie, P., Avallone, G., De Gregorio, F., Romano, G. P., & Antonia, R. A. (2007). Spatial resolution of PIV for the measurement of turbulence. *Experiments in Fluids*, *43*, 39–51. doi:10.1007/s00348-007-0319-x.

Lee, E. S., Ranasinghe, D. R., Ahangar, F. E., Amini, S., Mara, S., Choi, W., Paulson, S., & Zhu, Y. (2018). Field evaluation of vegetation and noise barriers for mitigation of near-freeway air pollution under variable wind conditions. *Atmospheric Environment*, *175*, 92–99. doi:10.1016/j.atmosenv.2017.11.060.

Meroney, R. (2004). Wind tunnel and numerical simulation of pollution dispersion: a hybrid approach. *Paper for Invited Lecture at the Croucher Advanced Study Institute, Hong Kong University of Science and Technology*, . URL: http://www.engr.colostate.edu/~meroney/PapersPDF/CEP04-05-2.pdf.

Morawska, L., Ristovski, Z., Jayaratne, E., Keogh, D. U., & Ling, X. (2008). Ambient nano and ultrafine particles from motor vehicle emissions: Characteristics, ambient processing and implications on human exposure. *Atmospheric Environment*, *42*, 8113–8138. doi:10.1016/j.atmosenv.2008.07.050.

Nabielek, K., Kronberger-Nabielek, P., & Hamers, D. (2013). The rural-urban fringe in the Netherlands: recent developments and future challenges. *Spool*, *1*, 101–120. URL: http://ojs-lib.tudelft.nl/index.php/spool/article/view/624.

Oke, T. (1988). Street design and urban canopy layer climate. *Energy and Buildings*, *11*, 103 – 113. doi:10.1016/0378-7788(88)90026-6.

Pope III, C., Burnett, R., Thun, M., Calle, E. E., Krewski, D., Ito, K., & Thurston, G. D. (2002). Lung cancer, cardiopulmonary mortality, and long-term exposure to fine particulate air pollution. *JAMA*, *287*, 1132–1141. doi:10.1001/jama.287.9.1132.

Pope III, C. A., & Dockery, D. W. (2006). Health effects of fine particulate air pollution: Lines that connect. *Journal of the Air & Waste Management Association*, *56*, 709–742. doi:10.1080/10473289.2006.10464485.

Pournazeri, S., & Princevac, M. (2015). Sound wall barriers: Near roadway dispersion under neutrally stratified boundary layer. *Transportation Research Part D: Transport and Environment*, *41*, 386 – 400. doi:10.1016/j.trd.2015.09.025.

Pugh, T. A. M., MacKenzie, A. R., Whyatt, J. D., & Hewitt, C. N. (2012). Effectiveness of Green Infrastructure for Improvement of Air Quality in Urban Street Canyons. *Environmental Science & Technology*, *46*, 7692–7699. doi:10.1021/es300826w.

Schulte, N., Snyder, M., Isakov, V., Heist, D., & Venkatram, A. (2014). Effects of solid barriers on dispersion of roadway emissions. *Atmospheric Environment*, *97*, 286 – 295. doi:10.1016/j.atmosenv.2014.08.026.

Snyder, W. H. (1972). Similarity criteria for the application of fluid models to the study of air pollution meteorology. *Boundary-Layer Meteorology*, *3*, 113–134. doi:10.1007/BF00769111.

Steffens, J. T., Heist, D. K., Perry, S. G., Isakov, V., Baldauf, R. W., & Zhang, K. M. (2014). Effects of roadway configurations on near-road air quality and the implications on roadway designs. *Atmospheric Environment*, *94*, 74 – 85. doi:10.1016/j.atmosenv.2014.05.015.

Steffens, J. T., Heist, D. K., Perry, S. G., & Zhang, K. M. (2013). Modeling the effects of a solid barrier on pollutant dispersion under various atmospheric stability conditions. *Atmospheric Environment*, *69*, 76 – 85. doi:10.1016/j.atmosenv.2012.11.051.

Stull, R. (2016). *Practical Meteorology: an algebra based survey of atmospheric science*. BC Campus. URL: http://doer.col.org/handle/123456789/5710.

Takano, Y., & Moonen, P. (2013). On the influence of roof shape on flow and dispersion in an urban street canyon. *Journal of Wind Engineering and Industrial Aerodynamics*, *123*, 107 – 120. doi:10.1016/j.jweia.2013.10.006.

Teunissen, H. (1970). *Characteristics of the mean wind and turbulence in the planetary boundary layer*. Technical Report Toronto University Downsview (Ontario) Institute for Aerospace studies. URL: www.dtic.mil/get-tr-doc/pdf?AD=AD0722047.

Tomas, J., Eisma, H., Pourquie, M., Elsinga, G., Jonker, H., & Westerweel, J. (2017). Pollutant dispersion in boundary layers exposed to rural-to-urban transitions: Varying the spanwise length scale of the roughness. *Boundary-Layer Meteorology*, *163*, 225–251. doi:10.1007/s10546-016-0226-x.

Tominaga, Y., & Stathopoulos, T. (2016). Ten questions concerning modeling of near-field pollutant dispersion in the built environment. *Building and Environment*, *105*, 390 – 402. doi:10.1016/j.buildenv.2016.06.027.

Vanderwel, C., & Tavoularis, S. (2014). On the accuracy of PLIF measurements in slender plumes. *Experiments in fluids*, *55*, 1801. doi:10.1007/s00348-014-1801-x.

Wilson, J. F., Cobb, E. D., & Kilpatrick, F. A. (1986). *Fluorometric procedures for dye tracing*. Department of the Interior, US Geological Survey. URL: http://www.comm-tec.com/library/technical_papers/usgs/twri_3-a12.pdf.

World Health Organization (2006a). *Air quality guidelines: global update 2005: particulate matter, ozone, nitrogen dioxide, and sulfur dioxide*. World Health Organization. URL: http://www.euro.who.int/__data/assets/pdf_file/0005/78638/E90038.pdf?ua=1.

World Health Organization (2006b). *Health risks of particulate matter from long-range transboundary air pollution*. Copenhagen: WHO Regional Office for Europe. URL: http://www.euro.who.int/__data/assets/pdf_file/0006/78657/E88189.pdf.

Yassin, M. F. (2011). Impact of height and shape of building roof on air quality in urban street canyons. *Atmospheric Environment*, *45*, 5220 – 5229. doi:10.1016/j.atmosenv.2011.05.060.